J Solid State Electrochem (2011) 15:579–585
DOI 10.1007/s10008-010-1130-9

ORIGINAL PAPER

Activated carbon prepared from polyaniline base by K_2CO_3 activation for application in supercapacitor electrodes

Xiaoxia Xiang · Enhui Liu · Limin Li · Yanjing Yang · Haijie Shen · Zhengzheng Huang · Yingying Tian

Received: 9 February 2010 / Revised: 14 June 2010 / Accepted: 14 June 2010 / Published online: 25 June 2010

Abstract An activated carbon was prepared from a polyaniline base using K_2CO_3 as an activating agent. The morphology, surface chemical composition, and surface area of the as-prepared carbon materials were investigated by scanning electron microscope, X-ray photoelectron spectroscopy, and Brunauer–Emmett–Teller measurement, respectively. Electrochemical properties of the as-prepared sample were studied by cyclic voltammetry, galvanostatic charge/discharge, and electrochemical impedance spectroscopy measurements in 6 mol L^{-1} KOH aqueous solution. Compared with the non-activated carbon, activated carbon showed superior capacitive performance. The activation carbon presented a high specific gravimetric capacitance of 210 F g^{-1}. The good electrochemical performance of the activated carbon was ascribed to well-developed micropores, high surface area, the presence of nitrogen and oxygen functional groups, and larger pore volume.

Keywords Supercapacitor · Polyaniline · Activated carbon · X-ray photoelectron spectroscopy · K_2CO_3

Introduction

Supercapacitors have attracted much attention because of their higher power density, better efficiency, and longer durability in comparison to the rechargeable batteries [1, 2]. Based on charge storage mechanisms, supercapacitors can be divided into electric double-layer capacitors (EDLCs) and redox pseudocapacitors [3].

In recent years, considerable attention has been paid to developing better electrode materials for supercapacitors. Among various electrode candidates for supercapacitors, porous carbons are mainly investigated due to their advantages such as good electrical conductivity, electrochemical stability, high surface area, large capacitance, long cycling life, and relatively low cost [4–6].

The choice of carbon precursor and activation conditions determines the device capacitive performance, such as carbon surface area, pore-size distribution, electrical conductivity, and the presence of electrochemically active surface functional groups [7]. The textural characteristics of carbons can be modified significantly by an activation process that removes the most reactive carbon atoms from the structure, thus increasing the surface area and porosity [8].

Broadly, two activation methods are used to prepare activated carbons: physical activation and chemical activation. In physical activation, the raw material is carbonized under an inert atmosphere and then activated at high temperature by using an activating reagent such as steam or CO_2 [9–11]. In chemical activation, the raw material is impregnated with an activation reagent and heated in an inert atmosphere. The carbonization step and the activation step proceed simultaneously. Chemical activation has been successfully applied to the production of activated carbons by using various chemical reagents, i.e., KOH, $ZnCl_2$, and H_3PO_4 [4–6, 12]. Recently, alkali carbonates such as K_2CO_3 have been used in order to prepare activated carbons with high specific surface area [13–15]. Generally, chemical activation is the preferred route because it achieves higher yields and larger surface areas, needs lower operating temperatures and less activation time, and is more cost-effective [4, 8, 12, 16].

X. Xiang · E. Liu (✉) · L. Li · Y. Yang · H. Shen · Z. Huang · Y. Tian
Key Laboratory of Environmentally Friendly Chemistry and Applications of Ministry of Education, College of Chemistry, Xiangtan University,
Hunan 411105, People's Republic of China
e-mail: liuenhui99@sina.com.cn

There are many reports about the preparation of activated carbon materials from various precursors by chemical activation with different activating agents. Nahm et al. [17] have prepared activated carbon from coffee shells by using $ZnCl_2$ activation as supercapacitors. Activated carbons derived from bituminous coal and cherry stones by using KOH activation have been reported [18, 19]. There are also some reports about activated carbon prepared from palm shell and waste biomass by using K_2CO_3 activation to study its adsorption capacities [13, 14].

In this paper, we have prepared activated carbon from polyaniline (PANI) base using K_2CO_3. PANI contains about 15% nitrogen and 79% carbon; it is commercially available and very cheap [20]. We believe that it is a promising nitrogen-containing material as precursor to preparing activated carbon for supercapacitors. Nitrogen-enriched carbons can be synthesized from suitable nitrogen rich precursors [21]. The presence of nitrogen functionalities can enhance the capacitance of carbon material by enhancing the carbon wettability and by pseudo-Faradaic reactions [22, 23]. To the best of our knowledge, synthesizing such an activated carbon material for supercapacitors in this way has not yet been reported. The aim of this work was to investigate the effect of specific surface area and nitrogen and oxygen functional groups on electrochemical performance of the activated carbon.

Experimental

Preparation of PANI base

PANI was prepared by the oxypolymerization method which was reported by Liu et al. [20]. The PANI obtained from the polymerization was added to excess of 1 mol L^{-1} ammonium hydroxide, and then the reaction was kept for 12 h at room temperature under vigorous stirring. Finally, the resulting PANI was filtered, washed, and dried at 100 °C for 48 h under vacuum condition.

Preparation of activated carbon materials

The PANI base was ground to small particle size by hand. It was mixed with the activating agent (K_2CO_3) in 150 ml distilled water. The weight ratio of PANI base to K_2CO_3 was 2:1. This mixture was then dried at 105 °C for 24 h to prepare the impregnated sample.

The impregnated material was heated at the rate of 4 °C min^{-1} from room temperature up to 600 °C under nitrogen flow. Then it was cooled back to the initial temperature. After activation, the sample was first washed with 1 mol L^{-1} H_2SO_4 solution to remove residual chemical reagent and then washed several times with hot distilled water until the filtrate became neutral. The washed samples were dried at 100 °C for 24 h to obtain the activated carbons. The prepared activated carbon was marked as CA. For comparison, a carbonized sample was prepared from PANI base without K_2CO_3. Otherwise, the preparative procedure was the same as that of CA. This sample was marked as CC.

The characterization of materials

Surface morphology was investigated by Hitachi S5200scanning electron microscopy (SEM). The Brunauer–Emmett–Teller (BET) specific surface area and pore volumes of activated carbons were calculated from the isotherms of nitrogen adsorption/desorption at 77 K (NOVA-2200, Quantachrome) by using the BET equation. Chemical surface composition was investigated by X-ray photoelectron spectroscopy (XPS) on an ESCALAB250 (VG Scientific, UK) using a monochromatic Al Kα excitation source. The sample charging was corrected by

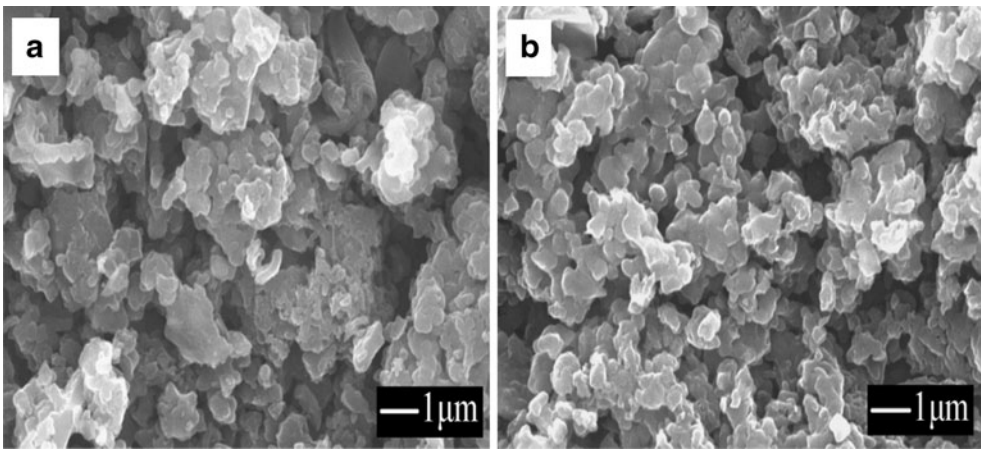

Fig. 1 SEM images of: **a** CC and **b** CA

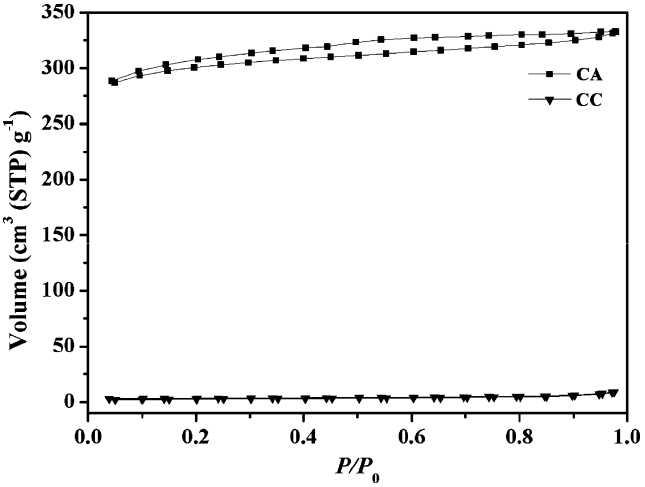

Fig. 2 N_2 adsorption/desorption isotherms of the CC and CA

using the C1s peak (Eb (C1s)=284.6 eV) as an internal standard. A non-linear, Shirley-type baseline and an iterative least-squares fitting algorithm were used to decompose the peaks; the best peak fits were obtained using mixed 20% Gaussian–Lorentzian. The surface atomic ratios were calculated from the ratio of the corresponding peak areas after correction with the theoretical sensitivity factors based on the Scofield's photoionization cross-sections.

Electrochemical test

The electrodes of the supercapacitors were prepared by pressing a mixture of 80 wt.% of as-prepared carbon, 10 wt.% of polivinylidene fluoride and 10 wt.% of acetylene black onto foamed nickel nets (diameter, 10 mm) and then drying in a vacuum oven at 110 °C overnight. Sandwich-type capacitors were constructed from two electrodes, with similar weights, facing each other, and separated by a nylon septum, in an aqueous electrolytic solution of 6 mol L^{-1} KOH. The electrochemical measurements were performed by means of a CHI 660A electrochemical workstation (CHI Inc., USA) at room temperature, and the capacitive performances were evaluated by cyclic voltammetry (CV), galvanostatic charge/discharge cycles, and electrochemical impedance spectroscopy (EIS). CV experiments was measured at scan rates ranging from 2 to 100 mV s^{-1}, galvanostatic charging/discharging cycles at current densities between 500 mA g^{-1} to 5 A g^{-1}, and EIS measurements were carried out by applying an AC voltage of 5 mV amplitude in the 100 kHz to 10 mHz frequency range.

Results and discussion

Characteristics of the carbon samples

Figure 1 shows the SEM images indicating the differences in the external surfaces of the CC and CA. It can be observed from the SEM that sample CC contains many large particles and, in general, exhibits an uneven distribution of particle sizes. The activation procedure caused a significant structural change. The CA particles are smaller and interconnect more densely than the CC particles. As expected, distinction in the surface morphology led to distinctions in the capacitive performance and the specific gravimetric capacitances of the samples.

The N_2 adsorption–desorption isotherms as shown in Fig. 2 are used to determine the surface area and pore-size distribution of the CA and CC. In the isotherm of CC, the adsorbed volume is very small, indicating its nonporous characteristics. The isotherm of CA exhibits type I characteristics exhibited by a well-defined plateau, according to IUPAC classification, which confirms its microporosity. An obvious hysteresis loop for CA is detected between the relative pressures (P/P_0) of 0.02 to 1. The hysteresis loop which persists to very low pressures is a low-pressure hysteresis (LPH). Vnukov et al. [24] showed that the broader the LPH loop, the greater the filling of the micropore volume.

Table 1 summarizes the textural properties of the samples. The CC sample possesses very low surface area (8.8 m^2 g^{-1}) because of its nonporous characteristics; however, the surface area of CA is very sharply increased through K_2CO_3 activation. Its value is as high as 917 m^2 g^{-1}. The CA has a low average pore diameter (1.39 nm) compared with the higher pore diameter (1.92 nm) of the CC. The micropores participate in the charge–storage processes by provide abundant adsorbing sites for the ions [10]. The higher the content of micropores, the higher the capacitance values obtained. In addition, the decomposition of potassium carbonate gives rise to K_2O and CO_2, which are reduced by

Table 1 Textural characteristics and specific capacitance of the CC and CA

Samples	Surface area, m^2 g^{-1}	Pore volume, cm^3 g^{-1}	Pore diameter, nm	C_{spec}, F g^{-1}
CC	8.9	0.011	1.92	35
CA	917	0.133	1.39	210

carbon to give K and CO. The proposed mechanism is shown below in Eqs. 1 and 2 [8]:

$$K_2CO_3 + C \rightleftarrows K_2O + 2CO \quad (1)$$

$$K_2O + C \rightleftarrows 2K + CO \quad (2)$$

A proportion of the produced potassium will be intercalated between the graphitic layers or form graphite–potassium intercalation compounds. As a result, some graphitic structures will be destroyed and micropores generated [25]. Total pore volume of CA (0.133 $cm^3\ g^{-1}$) is more than ten times higher than that of CC (0.011 $cm^3\ g^{-1}$).

XPS spectra of investigated carbons indicate the presence of three distinct peaks due to carbon, nitrogen, and oxygen in Fig. 3. The high-resolution O1s spectra reveal the presence of six peaks [22, 26–28] corresponding to C=O groups (peak 1, BE=530.4–530.8 eV), carbonyl type groups and/or quinone (peak 2, BE=531.0–531.1 eV), C–OH and/or C–O–C groups (peaks 3, 4, and 5, BE=532, 532.4–533.1 and 533.4 eV) and chemisorbed oxygen and/or water (peak 6, BE=534.8–535.6 eV). The Cls spectra of the samples have been resolved into five individual component peaks [26, 27, 29] representing graphitic carbon (peak 1, BE=284.6–285.1 eV), C–O and C–OH groups (peak 2, BE=285.8–285.9 eV), carbon present in alcohol or ether groups (peak 3, BE=286.3–287.0 eV), carbonyl groups or ether (peak 4, BE=287.5–288.1 eV), HO–C=O groups (peak 5, BE=288.9 eV). The peaks in the 286.3–287.5 eV regions may also have resulted from the presence of C–N structures. The Nls regions indicate the presence of several different species on each carbon. The peaks with higher binding energies can be ascribed to N-6 (pyridine-like structures; peak 1, BE=398.4–398.8 eV), N-5 (pyrrolic and pyridonic) or amine moieties (peak 2, BE=400.1–400.4 eV), N–Q (nitrogen substituents in the aromatic graphene structures–quaternary nitrogen; peak 3, BE=401.1–401.7 eV), pyridine-*N*-oxides or ammonia (peak 4, BE=402.1–402.6 eV) [26, 27, 30]. Compared with the sample CC, activation of the PANI base using K_2CO_3 as activating reagent led to an increase in the concentration of surface oxygen functional groups and a change in their distribution. The ratio of carbonyl type groups to C–OH and/or C–O–C groups increases.

Types of nitrogen surface functional groups are presented in Table 2. A comparison of the nitrogen-enriched carbons has shown that although they have almost the same content of nitrogen on the surface, the types and contribution of particular nitrogen species on their surfaces differ significantly. The nitrogen of CC sample occurs in the form of three species: 66.81% of the total nitrogen on the surface is the N-5 type and 31.59% is

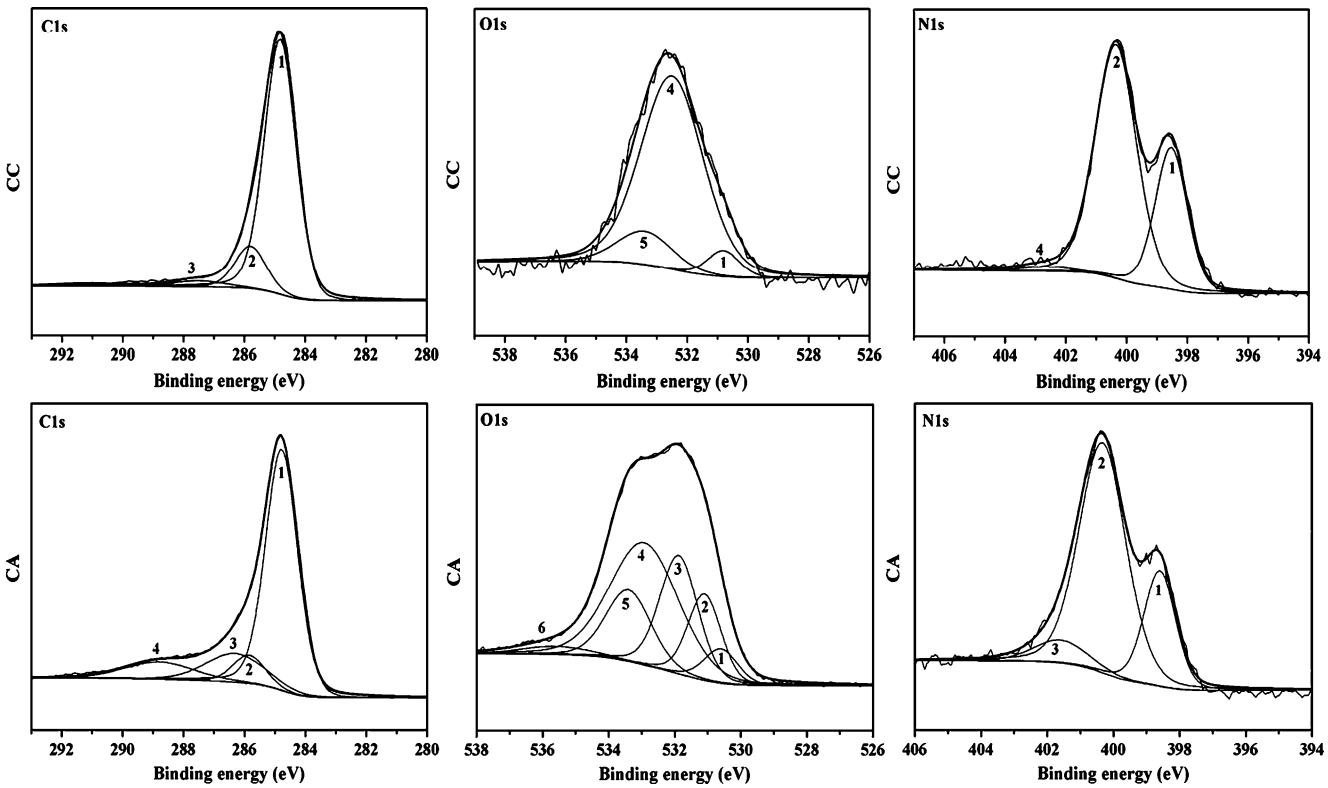

Fig. 3 X-ray photoelectron spectra of the CC and CA

Table 2 Surface composition and nitrogen form distribution in CC, CA

Sample	Atomic concentration						Nitrogen form distribution			
	C	N	O	N/C	O/C	N/O	N-6	N-5	N–Q	N–X
CC	75.58	18.7	5.71	0.247	0.076	3.275	31.59	66.81	–	1.60
CA	64.05	15.34	20.61	0.239	0.322	0.744	23.31	68.90	7.79	–

the N-6 type, and the remaining 1.60% occurs as pyridine-*N*-oxides or ammonia. The dominant nitrogen species in the CA sample is also N-5 but its contribution reaches 68.90% while only 23.31% is of the N-6 type. The Nls spectrum also indicates that activating either destroys surface pyridine-like functional groups or transforms them into pyrrolic and pyridonic species. A small amount (7.79%) of N–Q (nitrogen substituents in the aromatic grapheme structures–quaternary nitrogen) is found in CA. The appeared of N–Q is followed by disappearance of pyridine-*N*-oxide species.

Electrochemical properties

The CV curves for CA and CC at a scan rate of 2 mVs^{-1} are presented in Fig. 4a. The CA shows a quasi-rectangular voltammogram shape at the low scan rate, indicative of a good candidate as electrode material for supercapacitors. The area of the CV curves in CA is obviously larger than that of CC in Fig. 4a, which means that the capability of charge loading and releasing for CA is larger than in CC. Moreover, the effects of voltage scan rates on the capacitive behavior of the CA were also investigated. Figure 4b shows CV results for sample CA at various scan rates. At 2, 5, and 10 mV s^{-1}, the curves present the rectangle shapes for the charge/discharge processes. At higher scan rate, for example, at 20 mV s^{-1}, a rectangular shape with only slight distortion can be seen. The specific gravimetric capacitances were calculated from the CV process of the sixth cycle on the basis of Eq. 3.

$$C_{\text{spec}} = \frac{i}{m_{\text{e}} \frac{\Delta v}{\Delta t}} \tag{3}$$

Where C_{spec} is the specific gravimetric capacitance (farad per gram), i is the charge/discharge current (milliamperes), m_{e} is the mass of the activated carbon (milligrams), and $\frac{\Delta v}{\Delta t}$ is the scan rate (millivolts per second). The specific capacitance of the CA still remains as high as 182 F g^{-1} at the high scan rate of 20 mV s^{-1}, 86.7% of that measured at 2 mV s^{-1} (210 F g^{-1}). It suggests that, after the activation, more surface area of the carbon was accessible to electrolyte ions due to the improved wettability of the carbon and faster charge propagation [31]. This result is supported by the BET results. In addition, a small hump during the sweep at 0.2–0.5 V was clearly observed for CA, which is usually attributed to pseudo-Faradic reactions involving the quinone functional groups. The nitrogen functional groups, especially the pyrrolic and pyridinic nitrogen have been reported to be electrochemically active in the pseudo-Faradaic reactions [22].

Galvanostatic charge/discharge measurements are commonly used to test the performance of capacitors. Figure 5 shows galvanostatic charge/discharge curves of the CC and CA at a current density of 500 mA g^{-1} between 0 and 1.0 V in a 6.0 mol L^{-1} KOH electrolyte. It is clear that the IR

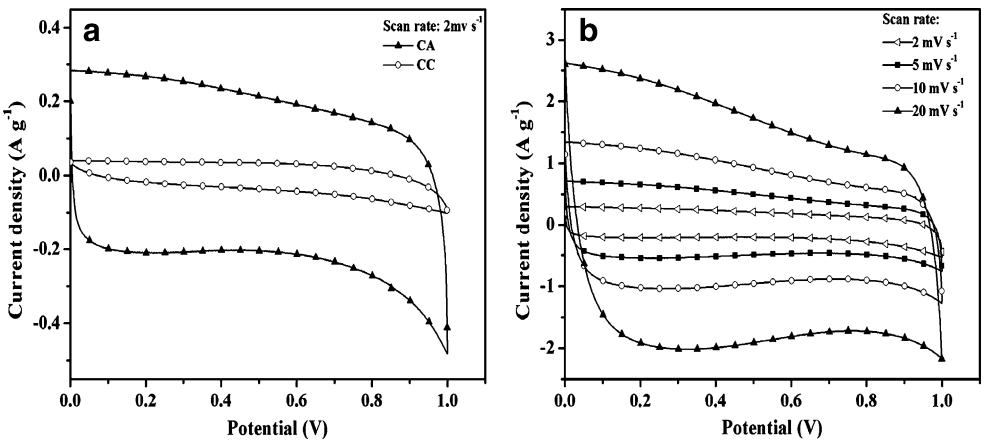

Fig. 4 Cyclic voltammograms of carbon electrodes in 6 mol L^{-1} KOH electrolyte, **a** the CC and CA at a scan rate of 2 mV s^{-1}, **b** the CA with different scan rates

drop, which can be observed from the discharge curves of the CC and CA, decreases after activation by K_2CO_3. The charge/discharge curves of CA approaches a triangular shape reflecting good charge/discharge capacitive performance. The specific gravimetric capacitances were calculated from the galvanostatic charge/discharge process on the basis of Eq. 4.

$$C_{\text{spec}} = \frac{i\Delta t}{m\Delta v} \tag{4}$$

Where C_{spec} is single-electrode specific gravimetric capacitance (farad per gram), i is the discharge current (milliamperes), Δt is the total discharge time (seconds), m is the total mass of active material in single-electrode (milligrams), and Δv is the potential difference during the discharging (volts). The specific capacitance of the CA reaches 199 F g^{-1}, much larger than that of the CC (19 F g^{-1}) under this current density. The higher capacitance of the CA can attribute to its higher specific surface area and larger pore volume.

In order to further understand the electrochemical performance, EIS measurements were conducted. The resistance of a supercapacitor, namely the equivalent series resistance (ESR), consists of electronic contributions and ionic contributions. The former refers to the intrinsic electronic resistance of the carbon particles and the interfacial resistances of particles-to-particles and particles-to-current collector. The latter is related to the electrolyte resistances in the pores, separator resistance and the ionic (diffusion) resistance of ions moving in small pores [6, 32]. Typical Nyquist impedance spectra recorded at a frequency range of 100 kHz to 10 mHz for CA and CC are shown in Fig. 6. At the very high-frequency region, the intercept at the real axis is the ESR. It

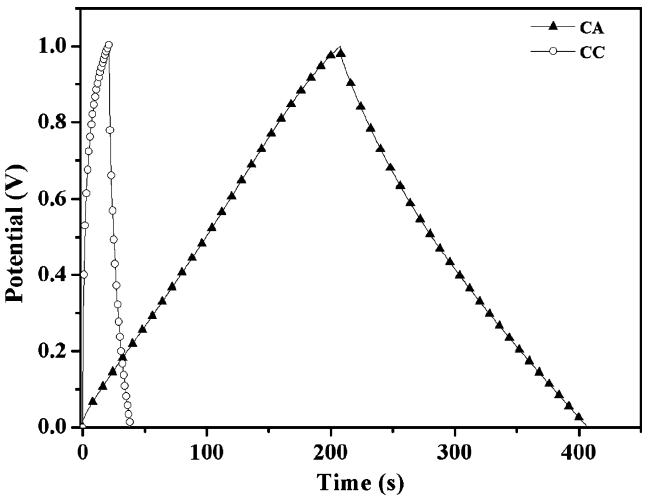

Fig. 5 Galvanostatic charge/discharge curves of the CC and CA at the current density of 500 mA g^{-1}

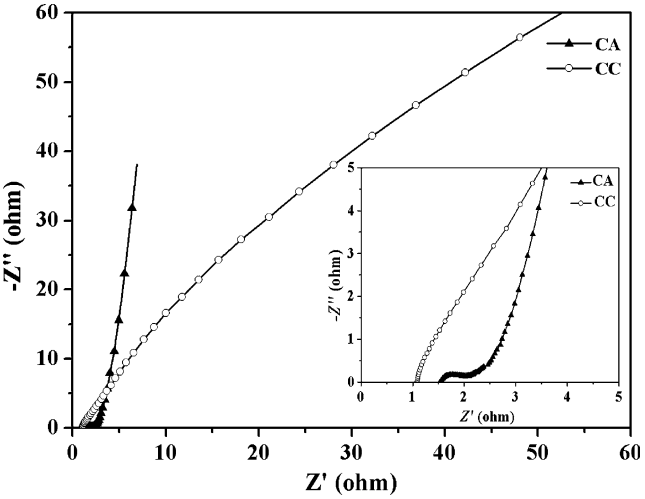

Fig. 6 Nyquist plot of the CC and CA (*inset*: enlarged high-frequency region of Nyquist plot)

can be seen that the ESR of CA (1.53 Ω) is higher than that of CC (1.09 Ω), indicating that the electric conductivity decreases. Jiang et al. [33] have reported that nitrogen functionalities can enhance the surface wettability and reduce the resistance of carbon. The nitrogen content of CA is lower than that of CC, so the electrical conductivity of CA is lower than that of CC. The depressed semicircle observed in the middle frequency range reveals the charge-transfer resistance (R_{ct}), which is 0.45 Ω for CA. This may be attributed to pseudo-Faradaic reactions involving the quinone functional groups. The straight line in both plots in the low frequency region reveals the capacitive nature of the carbons. The slope of the CA is steeper than that of the CC, which indicates that its capacitive performance is better. This is consistent with above results from CV and galvanostatic charge/discharge curves.

Conclusions

Electrode materials for supercapacitors were prepared from PANI base by K_2CO_3 activation. Compared with the CC, the K_2CO_3 activated carbon showed porous textures and remarkable enhancements in the specific surface area and volume of micropores. CA was superior to CC for the application of supercapacitors. The activated carbon CA exhibited the better electrochemical behavior with a specific gravimetric capacitance of 210 F g^{-1}, with rectangular cyclic voltammetry curves at a scan rate of 2 mV s^{-1}, which remained at 182 F g^{-1} even at a high scan rate of 20 mV s^{-1}. The good performance at high current loads is the obvious superiority of this kind of porous carbon over super-activated carbon. Correlating the capacitive behavior with textural characteristics, the good electrochemical

properties were ascribed to the narrow pore structure, high surface area, and larger pore volume.

Acknowledgement The authors are grateful for the project support by Hunan Provincial Natural Science Foundation of China (07JJ6015).

References

1. Zhou HH, Chen H, Luo SL, Lu GW, Wei WZ, Kuang YF (2005) J Solid State Electrochem 9:574–580
2. Lang JW, Kong LB, Liu M, Luo YC, Kang L (2009) Asymmetric supercapacitors based on stabilized α-Ni(OH)$_2$ and activated carbon. J Solid State Electrochem. doi:10.1007/s10008-009-0984-1
3. Wang YQ, Yuan AB, Wang XL (2008) J Solid State Electrochem 12:1101–1107
4. Kalpana D, Cho SH, Lee SB, Lee YS, Misra R, Renganathan NG (2009) J Power Sources 190:587–591
5. Rufford TE, Hulicova-Jurcakova D, Fiset E, Zhu ZH, Lu GQ (2009) Electrochem Commun 11:974–977
6. Wen ZB, Qu QT, Gao Q, Zheng XW, Hu ZH, Wu YP, Liu YF, Wang XJ (2009) Electrochem Commun 11:715–718
7. Rufford TE, Hulicova-Jurcakova D, Khosla K, Zhu ZH, Lu GQ (2010) J Power Sources 195:912–918
8. Jiménez V, Sánchez P, Valverde JL, Romero A (2009) J Colloid Interface Sci 336:712–722
9. Williams PT, Reed AR (2006) Biomass Bioenergy 30:144–152
10. Xia KS, Gao QM, Jiang JH, Hu J (2008) Carbon 46:1718–1726
11. Baçaoui A, Yaacoubi A, Dahbi A, Bennouna C, Luu RPT, Maldonado-Hodar FJ, Rivera-Utrilla J, Moreno-Castilla C (2001) Carbon 39:425–432
12. Liou TH, Wu SJ (2009) J Hazard Mater 171:693–703
13. Adinata D, Daud WMAW, Aroua MK (2007) Bioresour Technol 98:145–149
14. Tay T, Ucar S, Karagoz S (2009) J Hazard Mater 165:481–485
15. Hayashi J, Uchibayashi M, Horikawa T, Muroyama K, Gomes VG (2002) Carbon 40:2747–2752
16. Pandolfo AG, Hollenkamp AF (2006) J Power Sources 157:11–27
17. Jisha MR, Hwang YJ, Shin JS, Nahm KS, Kumar TP, Karthikeyan K, Dhanikaivelu N, Kalpana D, Renganathan NG, Stephan AM (2008) Mater Chem Phys 115:33–39
18. Zhang CX, Long DH, Xing BL, Qiao WM, Zhang R, Zhan L, Liang XY, Ling LC (2008) Electrochem Commun 10:1809–1811
19. Olivares-Marín M, Fernández JA, Lázaro MJ, Fernández-González C, Macías-García A, Gómez-Serrano V, Stoeckli F, Centeno TA (2009) Mater Chem Phys 114:323–327
20. Li LM, Liu EH, Li J, Yang YJ, Shen HJ, Huang ZZ, Xiang XX, Li W (2010) J Power Sources 195:1516–1521
21. Seredych M, Hulicova-Jurcakova D, Lu GQ, Bandosz TJ (2008) Carbon 46:1475–1488
22. Rufford TE, Hulicova-Jurcakova D, Zhu ZH, Lu GQ (2008) Electrochem Commun 10:1594–1597
23. Frackowiak E (2007) Phys Chem Chem Phys 9:1774–1785
24. Vnukov SP, Uspenskaya KS (1990) Phys Chem 1:7–10
25. Niu JJ, Wang JN (2008) Solid State Sci 10:1189–1193
26. Biniak S, Szymański G, Siedlewski J, Świątkowski A (1997) Carbon 35:1799–1810
27. Jurewicz K, Babeł K, Pietrzak R, Delpeux S, Wachowska H (2006) Carbon 44:2368–2375
28. Figueiredo JL, Pereira MFR, Freitas MMA, Órfão JJM (1999) Carbon 37:1379–1389
29. Li MH, Boggs M, Beebe TP, Huang CP (2008) Carbon 46:466–475
30. Pietrzak R (2009) Fuel 88:1871–1877
31. Fang BZ, Binde L (2006) J Phys Chem B 110:7877–7882
32. zKim C, Park SH, Lee WJ, Yang KS (2004) Electrochim Acta 50:877–881
33. Li WR, Chen DH, Li Z, Shi YF, Wan Y, Wang G, Jiang ZY, Zhao DY (2007) Carbon 45:1757–1763